JACS
JOURNAL OF THE AMERICAN CHEMICAL SOCIETY

Article

pubs.acs.org/JACS

Construction and Structure Determination of a Three-Dimensional DNA Crystal

Chad R. Simmons,[†,‡] Fei Zhang,[†,‡] Jens J. Birktoft,[§] Xiaodong Qi,[†,‡] Dongran Han,[†,‡] Yan Liu,[†,‡] Ruojie Sha,[§] Hatem O. Abdallah,[§] Carina Hernandez,[§] Yoel P. Ohayon,[§] Nadrian C. Seeman,*[,§] and Hao Yan*[,†,‡]

[†]Biodesign Center for Molecular Design and Biomimetics and [‡]School of Molecular Sciences, Arizona State University, Tempe, Arizona 85287, United States

[§]Department of Chemistry, New York University, New York, New York 10003, United States

Supporting Information

ABSTRACT: Structural DNA nanotechnology combines branched DNA junctions with sticky-ended cohesion to create self-assembling macromolecular architectures. One of the key goals of structural DNA nanotechnology is to construct three-dimensional (3D) crystalline lattices. Here we present a new DNA motif and a strategy that has led to the assembly of a 3D lattice. We have determined the X-ray crystal structures of two related constructs to 3.1 Å resolution using bromine-derivatized crystals. The motif we used employs a five-nucleotide repeating sequence that weaves through a series of two-turn DNA duplexes. The duplexes are tied into a layered structure that is organized and dictated by a concert of four-arm junctions; these in turn assemble into continuous arrays facilitated by sequence-specific sticky-ended cohesion. The 3D X-ray structure of these DNA crystals holds promise for the design of new structural motifs to create programmable 3D DNA lattices with atomic spatial resolution. The two arrays differ by the use of four or six repeats of the five-nucleotide units in the repeating but statistically disordered central strand. In addition, we report a 2D rhombuslike array formed from similar components.

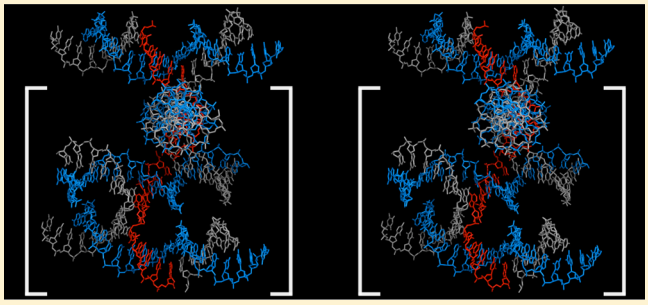

INTRODUCTION

Structural DNA nanotechnology has emerged as a prominent field that uses DNA as a molecular building block for programmable self-assembly. DNA possesses a number of attributes that make it ideally suited to address the challenges inherent in structural studies. It is a highly programmable polymer because Watson−Crick base pairing allows one to predict its secondary structure not only in linear molecules but also in branched molecules.[1] In addition, intermolecular interactions can be controlled via sticky-ended cohesion, which permits programming of the affinity between molecules in the context of a well-defined local product structure that is known a priori.[2,3] These properties have enabled its use to form designed self-assembled periodic lattices in two[4] and three dimensions.[5−7] In addition, one of the major motivating factors for the advent of the field was the ability of DNA to serve as a material that can be used to organize precisely a host of other chemical species, ranging from small molecules and peptides to nanoparticles, proteins, and viruses.[8−14]

Periodic two-dimensional (2D) self-assembling arrays have been demonstrated using a variety of DNA motifs, including the DNA double crossover (DX),[15,16] triple crossover (TX),[17] and DX and TX DNA triangles,[18,19] among many other examples.[20−26] Nevertheless, to date the only motif used successfully to self-assemble into crystals that diffract according to design and to a useful resolution is the "tensegrity triangle".[5] The tensegrity triangle yielding the highest-resolution 3D crystals contains two turns of DNA in each edge, with seven nucleotide pairs between crossovers within the triangle. It is reasonable to ask whether related structures might also yield useful crystals. Evident parameters to vary are the intercrossover spacing and the number of edges. Here we report the design of a "tensegrity square" with five nucleotides per edge and a "tensegrity hexagon" with a similar design. However, although the originally designed square was fashioned closely after the tensegrity triangle, the resulting crystals reflected a uniquely packed structure by comparison that was contrary to the intended square design. The structures revealed a trigonally symmetric three-dimensional (3D) array that diffracted to 3.1 Å in both cases. We report here those crystal structures and discuss how the structure elucidation could lead us to a new strategy for the design of self-assembling 3D DNA crystal lattices.

Received: June 28, 2016
Published: July 22, 2016

© 2016 American Chemical Society

DOI: 10.1021/jacs.6b06508
J. Am. Chem. Soc. 2016, 138, 10047−10054

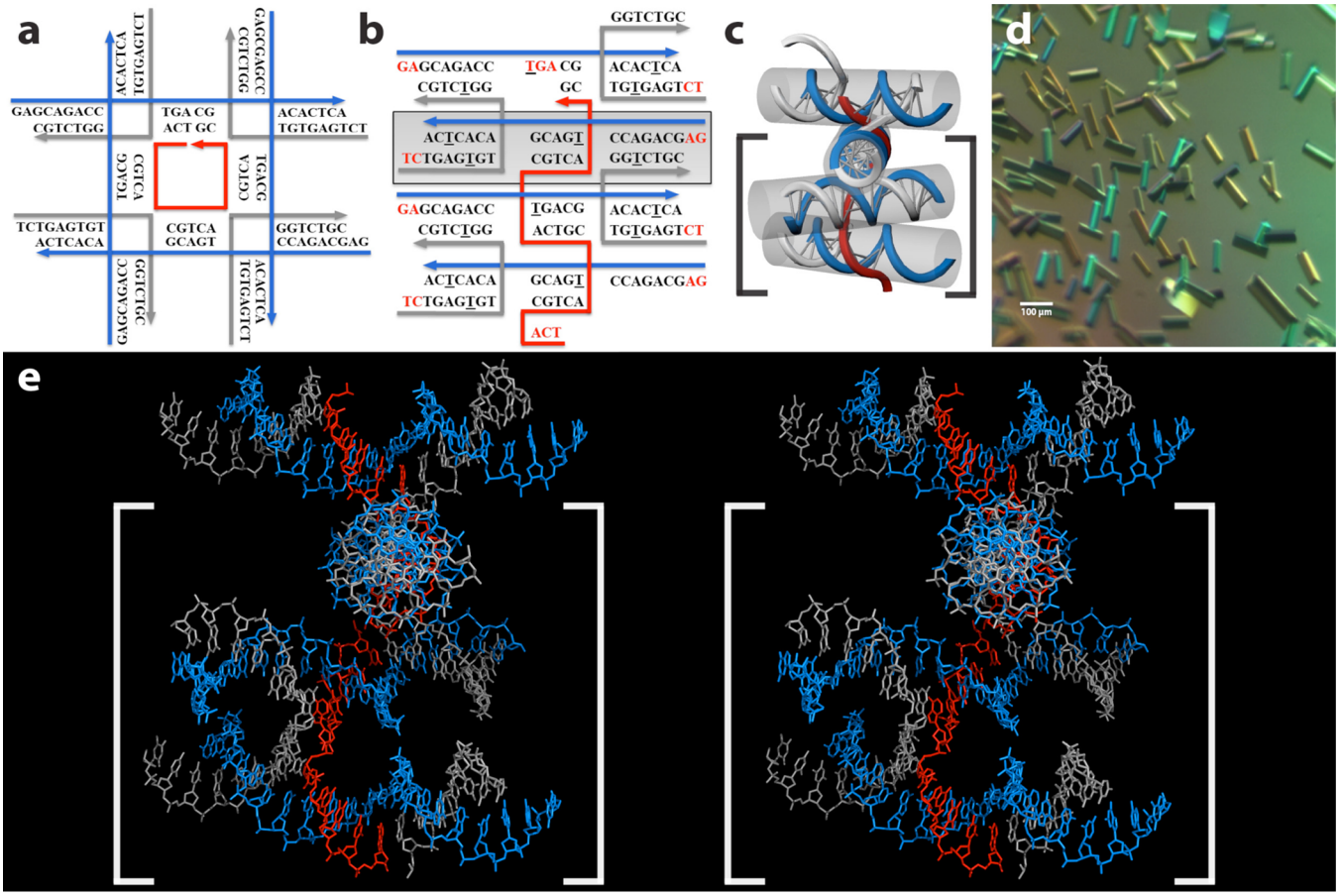

Figure 1. Schematic representation, model, crystals, and structure. (a) Topological representation of the initially designed square motif, which sought to use a central repeating strand (red) containing four identical sequence repeats to form a square unit flanked on each corner with a four-arm junction (blue and gray). (b) Schematic representation of the 4 × 5 structure, including the sequences used. The three component strands are represented in red (the central weaving strand), blue (a continuous single-stranded oligonucleotide constituting one half of the duplex in the ASU), and gray (flanking oligos forming junction crossovers flanking eight bases on each end of the main duplex). The ratio of strands required for the formation of the crystals is 1:4:4 (red:blue:gray). The arrowhead of each strand represents its 3′ end. The sticky ends used for hybridization are indicated with red letters. Each thymine position used for bromine derivatization is signified with an underlined letter. Each individual horizontal 21 bp helix represented constitutes one full ASU. One duplex has been outlined with a gray translucent box to highlight the sequence contributions to each helix in the ASU. (c) Cartoon depiction of the structure. Component strands are colored as shown in (a) and (b). Although the central weaving strand is responsible for tethering four helices together, constituting one "block", each block in the lattice contains only three stacked helices from any given individual unit cell contributing to two blocks per cell (denoted with black brackets). (d) Polarized light image of the triangular prism crystals. The 100 μm scale bar is indicated. (e) Stereoscopic view of the crystal structure from four individual asymmetric units all linked via the central red weaving strand. The component strands are represented with the same colors as shown in the topological representation. White brackets indicate the stacked helices contained within any given unit cell.

RESULTS AND DISCUSSION

Overall Structure. In this report, we describe a route for the construction of highly compact DNA lattices using various numbers of repeating sequences. The initial strategy we employed was to use a "square" motif that contained three component strands (Figure 1a), namely, a central oligonucleotide strand containing a 20-nucleotide sequence (red) with four sequence repeats of five nucleotides along with additional flanking strands that form four four-arm junctions at the corners of the central square motif; this motif is tailed with two nucleotide sticky-ended sequences on each arm, as shown in Figure 1a. Upon inspection of this designed motif with physical modeling, we realized that in order for the central strand to make the fourth connection required for the formation of the square, a total of two complete helical turns (21 base pairs (bp)) allowing for two full 360° rotations (10.5 bp/full turn) to result in a 5′ to 3′ end connection after a full 720°, would be required. As a result, the 20-base central sequence leaves the connection at the nick site of the motif short of this target requirement with an angle of ~686°. That angle is not tolerated here, so instead of squares the result is a series of "blocks" of duplexes tethered together by the central sequence, resulting in the scheme shown in Figure 1b, with the size of the block determined by the number of repeats of the sequence (Figure 1c). Crystals of two constructs were obtained and investigated. Sequences containing four and six identical repeats of five bases (4 × 5 and 6 × 5) on the central strand were employed, and the X-ray structures were determined (Figure 1d,e). The two crystal types were isomorphous to each other. The crystal structure of each revealed that it did indeed differ from the original two-dimensional topological square design (Figure 1b,c). Structural analysis also revealed that it is only the central repeating strand that mediates lattice formation, yielding identical topologies of the 4 × 5 and 6 × 5 structures (Figure S1). It is worth noting that in a companion experiment with a 4

DOI: 10.1021/jacs.6b06508
J. Am. Chem. Soc. 2016, 138, 10047−10054

Table 1. Data Collection and Refinement Statistics

	4 × 5 SAD[a]	4 × 5 native[b]	6 × 5 SAD[a]	6 × 5 native[b]
		Data Collection		
space group	$P3_221$	$P3_221$	$P3_221$	$P3_221$
resolution (Å)	50 − 3.05 Å	30 − 3.1 Å	50 − 3.1 Å	50 − 3.15 Å
cell dimensions				
a, *b*, *c* (Å)	68.3, 68.3, 60.17	67.9, 67.9, 59.3	68.5, 68.5, 59.4	67.9, 67.9, 58.8
α, *β*, *γ* (deg)	90, 90, 120	90, 90, 120	90, 90, 120	90, 90, 120
R_{merge}	0.082 (0.608)[c]	0.065 (0.342)	0.101 (0.451)	0.073 (0.24)
$I/\sigma I$	28.0 (2.5)	74.9 (3.0)	36.2 (4.3)	71.2 (19.1)
completeness (%)	100 (100)	99.4 (93.5)	100 (100)	99.7 (100)
redundancy	9.7 (9.7)	9.8 (7.0)	9.7 (9.9)	20.5 (17.7)
		Refinement		
resolution (Å)		30 − 3.1 Å		50 − 3.15 Å
no. of reflections		29781		59701
R_{work}/R_{free}		20.42/25.97		23.18/27.47
no. of atoms		855		855
DNA		853		853
ligand/ion		2		2
RMSDs				
bond lengths (Å)		0.0139		0.0041
bond angles (deg)		1.317		0.589

[a]Data were collected at beamline X25 at NSLS. [b]Data were collected at beamline 8.2.2 at ALS. [c]The value for the highest-resolution shell is shown in parentheses.

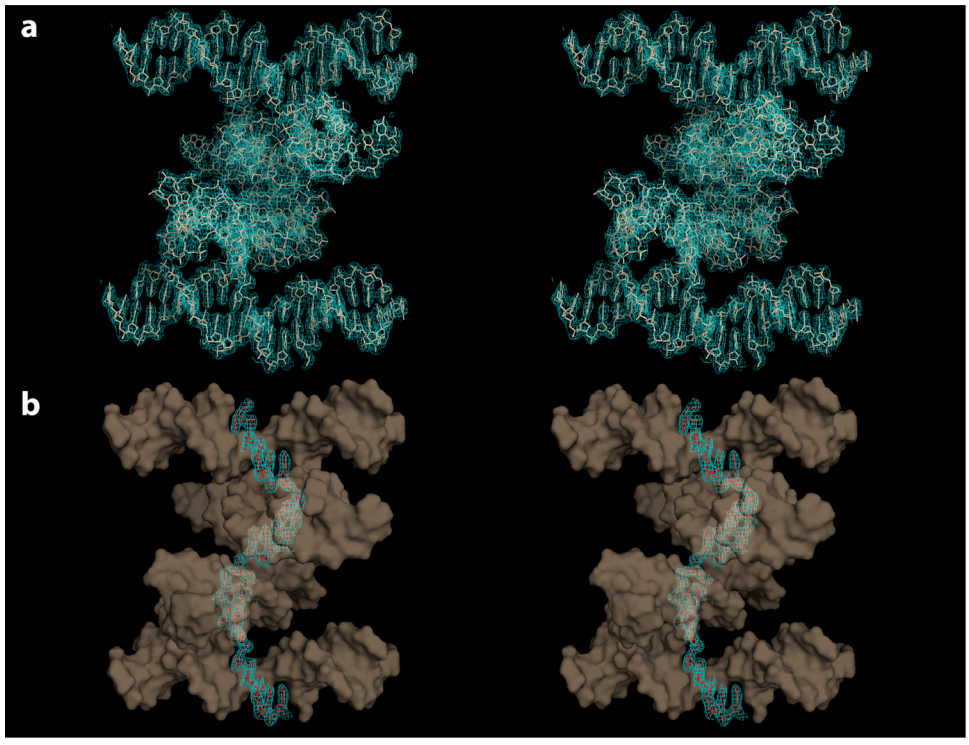

Figure 2. Crystal structure in electron density and the structural role of the central weaving strand. (a) $2F_o - F_c$ map (cyan) contoured at $\sigma = 1.5$ that was used for model building of the 4 × 5 structure. The stereoscopic view of the structure is oriented in the same manner as shown in Figure 1e. The major and minor grooves, phosphate backbone, and individual base stacking are readily observable (tan stick model). (b) Translucent stereoscopic surface rendering of the 4 × 5 structure (tan surface). The central weaving strand is shown with red sticks in the $2F_o - F_c$ map (cyan) contoured at $\sigma = 1.5$. The electron density for the weaving strand is readily observable across the junctions, and the built model is in very good agreement with the density.

× 7 design, a 2D rhombuslike lattice was the product, although a different buffer was used for that purpose (see below). The 3D structures contain three component oligonucleotide strands tailed by two-nucleotide sticky ends, allowing the duplexes to self-associate into continuous arrays of 21-nucleotide-pair helices traveling in each of the three directions in accord with the crystallographic threefold screw (3_2) symmetry. Thus, the motif contains the original sequences used in the initial square design, but the central (red) strand, apparently disordered, weaves through and connects the 21 nucleotide pair duplexes in

DOI: 10.1021/jacs.6b06508
J. Am. Chem. Soc. 2016, 138, 10047−10054

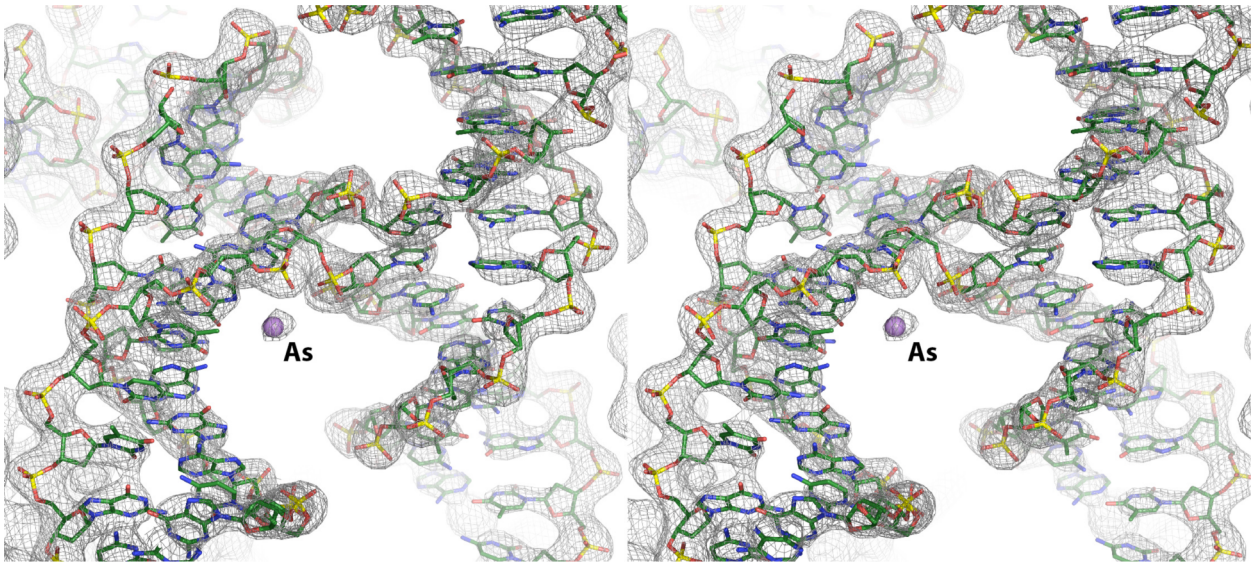

Figure 3. Structure of the Holliday junction. Stereoview of a four-arm junction contained in the $2F_o - F_c$ map contoured at $\sigma = 1.5$. The portion of the structure shown here demonstrates the quality of the fit of the model to the density and shows the two junction connections made across the borders between adjacent asymmetric junctions. The 120° angle adopted by a standard junction is readily observable. The stick representation is colored with atoms represented as follows: carbons (green), phosphates (yellow), oxygens (red), and nitrogens (blue). Only a single peak of residual density exists within each junction site and has been taken into account by an As ion (magenta sphere; for details, see the text and Figure S4). No remaining interpretable density is observable within the unit cell.

each asymmetric unit (ASU). See below for further discussion of this issue.

The bromine positions used for phasing the crystals are indicated, with their corresponding nucleotides underlined in Figure 1b. Each ASU was refined as containing a single 21 nucleotide strand (blue) paired in standard B-DNA fashion with a five-nucleotide sequence at its center flanked by two eight-nucleotide pair regions (gray). Bromine-derivatized crystals (four Br per ASU) were employed for an independent set of phases for each case to provide unbiased structure determinations (additional details regarding crystallographic phase determination are described below). Each structure crystallized in space group $P3_221$ with unit cell dimensions $a = b = 68$ Å, $c = 59$ Å, $\alpha = \beta = 90°$, and $\gamma = 120°$. All of the data processing and refinement statistics are reported in Table 1. The unit cell volume is ~232 000 Å^3, with a solvent content of approximately 55%, indicating a fairly densely packed atomic environment. The unit cell contains six ASUs in space group $P3_221$ with a total of 21 nucleotide pairs contained within each ASU. The crystal structure is best described in each case as a grouping of double helices oriented 120° from their adjacent partners, facilitated by a four-arm junction at five-nucleotide intervals until its termination at its 3′ end, at which point the next repeating oligonucleotide continues the series constituting the lattice. In this example, we depict the topological structure of the 4 × 5 crystal as a series of three duplexes, with the three component strands colored according to their locations in the resulting crystal structure (Figure 1e). Each resulting crystal structure is in very good agreement with the electron density at 3.1 Å resolution (Figure 2a). Since a single block contains four tethered duplexes, the total unit cell contains 1.5 blocks per cell with the 4 × 5 motif. The resulting structure reveals double helices of standard B-DNA, where structural details can be resolved clearly. These include the major and minor grooves, a very clear trace of the phosphate backbones, clearly resolved base-pair stacking, C2′-endo nucleoside conformations, and the weaving of the central five-nucleotide repeating sequence connecting each ASU (Figures 1e and 2a). The 4 × 5 structure shown here contains three duplexes connected via standard four-arm junctions, which dictate that they are oriented with a 120° rotation with respect to one another. This phenomenon results in a helical relationship of layers of duplexes solely facilitated by the repeating central sequence weaving through the layers of helices (Figure S2), with the central repeating sequence positioned well within its density (Figure 2b). It is clear that the central strand must be disordered for the 4 × 5 system to be in agreement with the space group symmetry. It is not possible to find the nick between neighboring central strands in the way that it is possible to find the nicks between the strands on the sticky ends. The 6 × 5 structure revealed details identical to those observed with the 4 × 5 system, and therefore, we will describe details that mainly apply to both structures.

Bromine-Derivatized Structures. The structures of both the 4 × 5 and 6 × 5 crystals were determined using independent sets of phases from bromine-derivatized crystals. Each two-turn duplex in the ASU contained four bromine atoms covalently linked to C5 of four thymine bases (bromo-dU). Anomalous difference Fourier maps were calculated and yielded four distinct peaks in the maps (Figure S3). The model was built from the resulting phases, with each of the bromine peaks in very good agreement with the positions indicated by the sequences in Figure 1b. Furthermore, two additional peaks were observed in the anomalous difference maps on two opposing corners of the four-arm junction, at equivalent positions in the two structures. Because the crystallization buffer contained cacodylic acid ($(CH_3)_2As(O)OH$) in both cases, we attempted to model the buffer molecule into the electron density at these positions. Although only a single peak was observed, accounting for the putative As atom position, the entire modeled cacodylate structure was reasonably well fit without any van der Waals clashes and furthermore was capable

DOI: 10.1021/jacs.6b06508
J. Am. Chem. Soc. 2016, 138, 10047−10054

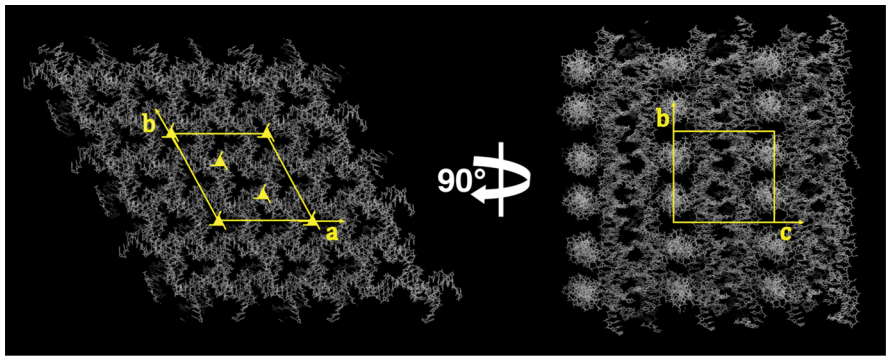

Figure 4. Crystal packing. Two orientations of the lattice are shown to demonstrate the crystal packing. (left) The unit cell is indicated in yellow for the crystal with space group $P3_221$ and unit cell dimensions $a = b = 68$ Å, $c = 59$ Å, $\alpha = \beta = 90°$, and $\gamma = 120°$. The threefold-symmetry screw axes are indicated. The $a = b = 68$ Å axis is shown with the $\gamma = 120°$ angle clear in this orientation. (right) View with a 90° rotation about the vertical axis with respect to the first view to demonstrate the $a = b = 68$ Å axis and $c = 59$ Å with $\alpha = \beta = 90°$. Continuous arrays of helices (or blocks of helices) constitute the structure, which are facilitated via sticky end cohesion and are oriented at 120° angles with respect to one another via the four-arm junction connections.

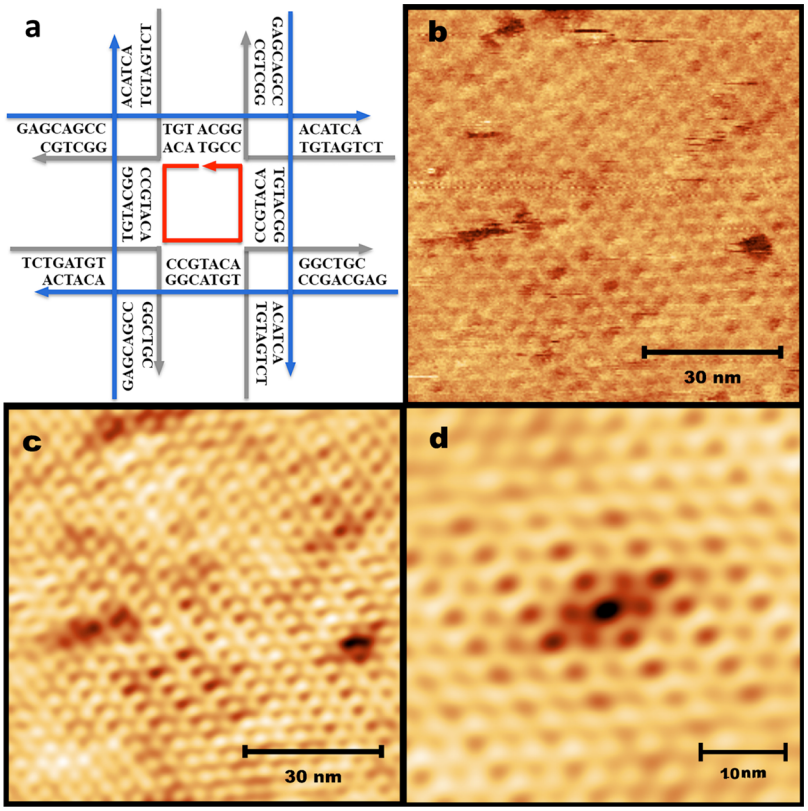

Figure 5. The 2D lattice with the seven-nucleotide spacing. (a) Schematic of the design. (b) Raw AFM image of the lattice generated by the system. (c) Fourier-flattened image of (b). (d) Autocorrelation function of (c). A translational repeat corresponds to a small rhombus (corresponding to the red line) followed by the large rhombus that comes from the inter-small-rhombus spacing. The two spacings are ~45 Å for the large separation and ~30 Å for the small separation, for a rough separation of 75 Å. The angle between the two directions is ~60°.

of being well-coordinated by polar contacts on each side of the junctions. Although data for the derivative crystals were collected at the bromine K edge (λ = 0.92 Å), the As absorption edge (λ = 1.04 Å) was still close enough to that wavelength to yield an anomalous signal, further substantiating the ion positions. No other components in the crystal mother liquor could either meet these criteria or account for the observed difference density. The arsenate positions in the 4 × 5 and 6 × 5 structures were equivalent.

Modeling Four-Arm Junctions between Duplexes. As discussed above, the initial 21 bp duplex was built using the phases determined from the bromine positions, but during subsequent rounds of refinement we were careful to focus upon refinement of all atoms in the ASU. We took great care to avoid introducing any inherent model bias into the geometry of the junctions at each of the connections. Later, we redefined the ASU as a single 21 bp four-arm junction (10 and 11 nucleotide pairs on either side of the junction) and modeled the connected duplexes into the clear junctions in the $2F_o - F_c$ density map (Figure 3). This structure was then energy-minimized for both geometry and angular orientations using the parameters originally described by Ho and colleagues[27] and those used

DOI: 10.1021/jacs.6b06508
J. Am. Chem. Soc. 2016, 138, 10047−10054

in the initial report of the tensegrity triangle.[5] After the refinement was complete, the junctions were clearly confined properly to the electron density, while the bond lengths and bond angles conformed to expectations.

Structural Ramifications of the Central Component Strand. The sole facilitators of the continuous helical arrays in the crystal are the two-nucleotide sticky ends placed on each end of each duplex on each of the levels of the structure. The single determinant for the attachments across each linear duplex is the repeating sequence weaving through them, leading to the frequently observed 120° angle dictated by each four-arm junction, first noted in the structures of Timset et al.[28] Between the two structures reported here, the most important distinction is the number of helical arrays that are attached from the 5′ end to the 3′ end of each strand. Whether there are four or six repeats in the central strand, each block is established with a thickness that is determined by the fundamental 120° screw rotational relationship between double helices. Each series of blocks in the crystal orients itself to pack with threefold screw symmetry relative to one another, with the edges of each resulting cavity along the threefold axis shown in Figure 4 being ∼3.4 nm in length. Furthermore, as the unit cell constants indicate, two-helical-turn duplexes (21 bp, 68 Å) oriented in $a = b = 68$ Å with respect to one another allow the crystal to pack in a series of layered duplexes, as demonstrated in the two additional orientations shown (Figure 4), and with $c = 58$ Å resulting from three layered helices with a diameter of ∼20 Å per duplex. The densely packed environment shown here clearly demonstrates the significant exclusion of solvent exerted by the compact arrangement of the four-arm junctions.

Our description of the electron density is most certainly not compatible with the components present in a simple way. By refining the 4 × 5 structure with a c axis around 3 times the thickness of a double helix, we have assumed implicitly that the central strand in both structures suffers from statistical disorder of one form or another. One might ask instead whether the 6 × 5 structure is indeed twice as long in the c direction as we describe (Figure S4), with very faint reflections in the intervening layers; similarly, the 4 × 5 structure might have a c axis triple the indicated length in its intervening layers (Figure S5). We tested this possibility by reprocessing the data to include the $l = 2n + 1$ layers corresponding to the doubled c axis of the 6 × 5 structure; likewise, we reprocessed the data to include the $l = 3n \pm 1$ layers corresponding to the tripled c axis of the 4 × 5 structure. We phased the few reflections we obtained by the structures we had, minimally refining the reflections. We looked to see whether we had clear gaps between the ends of the central strand (as we did in the transverse directions), indicating that we were indeed using the incorrect unit cell to describe the distribution of electron density within the crystal. Insofar as we could tell, nothing indicated that this was the case.

Two-Dimensional Lattice of a 4 × 7 Motif. The use of a 4 × 7 motif in this series resulted in a 2D arrangement of DNA that could be visualized by atomic force microscopy (AFM). This array is shown in Figure 5. Figure 5a is a schematic of the design, and Figure 5b displays the structure seen when the array is deposited on mica; Figure 5c presents a Fourier-cleaned image, and Figure 5d shows its autocorrelation function. The nonorthogonal arrangement of the molecular array is evident in these images, with the fundamental repeat being a rhombus with edge lengths of ∼60 Å and an angle of ∼60° between them, as shown in Figure 5d. Thus, it is possible to expand the number of sides in the motif from three to four to produce an array with periodicity in two dimensions. The 60° angle is similar to that in arrays produced earlier with branched junctions at their vertices.[29]

As mentioned above, the nucleotide deficit of the central strand for the 4 × 5 motif prevents it from completing two full helical turns, resulting in the layered arrangement instead of the originally designed square motif. However, by expanding the interjunction distance between four identical sequence repeats from five to seven nucleotides enables the formation of the 2D array (Figure 5). We posit that exactly two-thirds of a helical turn on each edge allows the formation of the square, as it does for the triangle in the original tensegrity triangle. Thus, 21 nucleotides for three helices or 28 nucleotides for a square apparently have the same low stresses on them.

CONCLUSIONS

The two examples of self-assembling DNA crystals reported here have provided a novel route toward the design of highly ordered DNA lattices. Each of these structures reveals a packed arrangement of crystalline blocks resulting in a regular periodic arrangement of duplexes that are related by crystal symmetry in a simple fashion. The two constructs here are both structurally well-defined with sufficient near-atomic detail to facilitate strategic positioning of guest molecules, although the unseen components of the disordered strands do complicate the issue. The modularity of the motif provides us with the ability to modify the design in a number of ways, including modification of interjunction distances to tune the lattice packing so as to accommodate larger guests. Of course, increasing these distances has resulted in worse resolution in other systems.[5]

We have seen above that changing the number of nucleotide pairs in the sections of the motif enables us to produce arrangements of nucleic acid materials, although they do not conform simply to replication of the initial motif. The central repeating weaving strand described here may have served as a scaffold to facilitate the lattice formation. This may lead to new design strategies for programming DNA molecules into self-assembling 3D crystals.

EXPERIMENTAL SECTION

Crystallization. DNA oligonucleotides were purchased as HPLC-purified from Integrated DNA Technologies (Coralville, IA) or synthesized by standard phosphoramidite techniques on an Applied Biosystems 394 DNA synthesizer. The synthesized oligonucleotides were removed, deprotected from the solid support, and purified via polyacrylamide gel electrophoresis (PAGE). The dried pellets were diluted to 300 μM in H_2O. A 10-fold dilution of S1 was then prepared in H_2O to a final concentration of 30 μM, and then 4 equiv of both S2 and S3 were added to the mixture. All of the sequences used for these structures are listed in the Supporting Information, where the positions of the bromine sites are also indicated. Sample preparation of both native and bromine-derivatized samples was performed using the sitting drop vapor diffusion method by combining 4.5 μL of the oligo mixture with 2.25 μL of reservoir solution for both the 4 × 5 and 6 × 5 systems. The 4 × 5 motif crystallized in 50 mM cacodylate buffer (pH 6.0) containing 20 mM $MgCl_2$, 1.0 mM spermine, and 15% ethanol, whereas the 6 × 5 crystals formed in 50 mM cacodylate buffer (pH 6.5) containing 100 mM $MgCl_2$, 1.0 mM hexaamminecobalt(III), and 2.0 M NaCl. Crystal trays were placed in a chilling incubator (Torrey Pines Scientific, Carlsbad, CA) set to 60 °C and allowed to equilibrate at this temperature for 1 h, and then the temperature was reduced to 25 °C at a rate of 0.3 °C/h, by which time fully grown (100 μm × 25 μm × 25 μm) crystals had formed with the appearance of triangular prisms. Crystals were then transferred with cryoloops

DOI: 10.1021/jacs.6b06508
J. Am. Chem. Soc. 2016, 138, 10047−10054

(Hampton Research) into a drop containing artificial mother liquor supplemented with 30% glycerol and allowed to incubate for 2−5 min before being cryocooled by plunging into a liquid nitrogen bath.

Data Collection, Processing, and Structure Solution. Crystallographic data collection for all of the native data reported here was performed at the Advanced Light Source (ALS) at Lawrence Berkeley National Laboratory at beamline 8.2.2, with an ADSC Q315R detector at λ = 1.0 Å. A total of 180 × 1° and 360 × 1° oscillation frames were collected for the native 4 × 5 and 6 × 5, respectively. All of the data were indexed, refined, integrated, and scaled using the HKL2000 package.[30] All of the crystals belonged to space group $P3_221$. The single-wavelength anomalous dispersion (SAD) data for the bromine-derivatized crystals were collected at the National Synchrotron Light Source (NSLS) at Brookhaven National Laboratory at beamline X25/X29 on a Pilatus 6M detector, and the Structural Biology Center at beamline 19-ID at the Advanced Photon Source (APS) on an ADSC Q315R detector at an energy of λ = 0.92 Å based on a fluorescence scan at the bromine K edge. An entire 360° sphere (1° oscillations) of data was collected for both the 4 × 5 and 6 × 5 repeat bromine-derivatized crystals, and phases were initially determined using *hkl2map*,[31] the software suite containing the *Shelxc/d/e* programs.[32,33] The resulting initial electron density maps from the SAD phases revealed very clear helices with resolvable major and minor grooves. The reflection data were then fed into the Python-based Hierarchical Environment for Integrated Xtallography (PHENIX)[34] suite to validate independently the initial substructure from *hkl2map*; the four bromine positions and the resulting substructure in the ASU were identified via the Hybrid Substructure Search (HySS) and AutoSol program in the PHENIX package. The Autobuild program SOLVE was then used for initial refinement and phase calculation, and an initial model was built using RESOLVE.[35] Manual model building was then performed in Coot,[36] and subsequent iterative rounds of refinement were performed using both phenix.refine and REFMAC.[37,38] Anomalous difference Fourier maps using the derivative data clearly revealed the four strongest peaks for the appropriate positions at the designed bromo-dU sites. Specifically, the 21 nucleotide pair duplex was treated as one rigid body during refinement, after which time real-space and *XYZ* coordinate refinement was performed against each of the data sets at 3.1 Å. In later rounds, atom occupancies and temperature factors were refined, followed by simulated annealing. Calculations of R_{free} for each of the data sets were based upon 5% of the unique reflections. During further refinement, the resulting $(F_o - F_c)$ difference maps were used to determine two additional peaks flanking opposite sides of each junction (situated diagonally from one another). The Holliday junction connections were not made to adjacent asymmetric units until the final stages of refinement so that there would be no introduction of model bias or ambiguity in the appropriate angles yielded by the structure during iterative rounds of refinement. In addition, arsenic atoms contained in the crystallization buffer were modeled into two large difference peaks flanking two sites at each junction situated diagonally from one another, and upon refinement of individual occupancies, these atoms accounted for all of the residual difference density. Final statistics for all of the refined models are given in Table 1. The atomic coordinates and structure factors for the completed models have been deposited in the Protein Data Bank with accession codes 5KEK and 5KEO. All of the figures were generated with PyMOL.[39]

Formation of 4 × 7 DNA Tiles and AFM Imaging. DNA strands were mixed in a volume of 100 μL at a concentration of 40 μM in a buffer solution containing 40 mM Tris-HCl (pH 8.0), 20 mM acetic acid, 2.5 mM EDTA, and 125 mM magnesium acetate. Two-dimensional arrays were obtained by quick annealing with a temperature gradient from 65 to 4 °C for 1 h. A 5 μL aliquot was then spotted on freshly cleaved mica (Ted Pella) and left to adsorb for 30 s. An additional 30 μL of 1× TAE-Mg^{2+} (125 mM) buffer was then added to both the mica and the liquid cell. AFM imaging was performed on a NanoScope IV (Digital Instruments) in buffer in tapping mode using Veeco's Sharp Nitride Lever (SNL) probe.

■ ASSOCIATED CONTENT

Supporting Information

The Supporting Information is available free of charge on the ACS Publications website at DOI: 10.1021/jacs.6b06508.

Data analysis and DNA structure design and sequences (PDF)

■ AUTHOR INFORMATION

Corresponding Authors

*hao.yan@asu.edu

*ned.seeman@nyu.edu

Notes

The authors declare no competing financial interest.

■ ACKNOWLEDGMENTS

Data were collected at The Berkeley Center for Structural Biology (BCSB), the National Synchrotron Light Source (NSLS), and the Structural Biology Center (SBC). The BCSB (BL 8.2.2) is supported in part by the NIH, National Institute of General Medical Sciences, and the HHMI. The Advanced Light Source is supported by the U.S. Department of Energy (DOE) under Contract DE-AC02-05CH11231. The NSLS (BL X25/29) is principally supported by the Offices of Biological and Environmental Research and Basic Energy Sciences of the DOE and by the National Center for Research Resources (P41RR012408) and the National Institute of General Medical Sciences (P41GM103473) of the NIH. The SBC (BL 19-ID) is part of the Advanced Photon Source, a DOE Office of Science User Facility operated for the DOE Office of Science by Argonne National Laboratory under Contract DE-AC02-06CH11357. The Yan lab was supported by Grants to H.Y. and Y.L. from the NSF (1360635 and 1334109), the ARO (W911NF-12-1-0420), and the NIH (R01GM104960). H.Y. was also supported by the Presidential Strategic Initiative Fund from Arizona State University. The Seeman laboratory was supported by the following grants to N.C.S.: EFRI-1332411 and CCF-1526650 from the NSF, MURI W911NF-11-1-0024 from the ARO, N000141110729 from the ONR, DE-SC0007991 from the DOE for DNA synthesis and partial salary support, and GBMF3849 from the Gordon and Betty Moore Foundation.

■ REFERENCES

(1) Seeman, N. C. *J. Theor. Biol.* **1982**, *99*, 237.

(2) Seeman, N. C. *J. Biomol. Struct. Dyn.* **1985**, *3*, 11.

(3) Qiu, H.; Dewan, J. C.; Seeman, N. C. J. *J. Mol. Biol.* **1997**, *267*, 881.

(4) Seeman, N. C. *Nature* **2003**, *421*, 427.

(5) Zheng, J.; Birktoft, J. J.; Chen, Y.; Wang, T.; Sha, R.; Constantinou, P. E.; Ginell, S. L.; Mao, C.; Seeman, N. C. *Nature* **2009**, *461*, 74.

(6) Liu, D.; Wang, W.; Deng, Z.; Walulu, R.; Mao, C. *J. Am. Chem. Soc.* **2004**, *126*, 2324.

(7) Wang, T.; Sha, R.; Birktoft, J. J.; Zheng, J.; Mao, C.; Seeman, N. C. *J. Am. Chem. Soc.* **2010**, *132*, 15471.

(8) Wilner, O.; Weizmann, Y.; Gill, R.; Lioubashevski, O.; Freeman, R.; Willner, I. *Nat. Nanotechnol.* **2009**, *4*, 249.

(9) Aldaye, F. A.; Palmer, A. L.; Sleiman, H. F. *Science* **2008**, *321*, 1795.

(10) Park, S. Y.; Lytton-Jean, A. K. R.; Lee, B.; Weigand, S.; Schatz, G.; Mirkin, C. A. *Nature* **2008**, *451*, 553.

(11) Sharma, J.; Ke, Y.; Lin, C.; Chhabra, R.; Wang, Q.; Nangreave, J.; Liu, Y.; Yan, H. *Angew. Chem., Int. Ed.* **2008**, *47*, 5157.

DOI: 10.1021/jacs.6b06508
J. Am. Chem. Soc. 2016, 138, 10047−10054

(12) Rinker, S.; Ke, Y.; Liu, Y.; Chhabra, R.l; Yan, H. *Nat. Nanotechnol.* **2008**, *3*, 418.
(13) Li, H.; Park, S. H.; Reif, J. H.; LaBean, T. H.; Yan, H. *J. Am. Chem. Soc.* **2004**, *126*, 418.
(14) Park, S. H.; Yin, P.; Liu, Y.; Reif, J. H.; LaBean, T. H.; Yan, H. *Nano Lett.* **2005**, *5*, 729.
(15) Winfree, E.; Liu, F.; Wenzler, L. A.; Seeman, N. C. *Nature* **1998**, *394*, 539.
(16) Li, X.; Yang, X.; Qi, J.; Seeman, N. C. *J. Am. Chem. Soc.* **1996**, *118*, 6131.
(17) Labean, T.; Yan, H.; Kopatsch, J.; Liu, F.; Winfree, E.; Reif, J. H.; Seeman, N. C. *J. Am. Chem. Soc.* **2000**, *122*, 1848.
(18) Zheng, J.; Constantinou, P. E.; Micheel, C.; Alivisatos, A. P.; Kiehl, R. A.; Seeman, N. C. *Nano Lett.* **2006**, *6*, 1502.
(19) Constantinou, P. E.; Wang, T.; Kopatsch, J.; Israel, L. B.; Zhang, X.; Ding, B.; Sherman, W. B.; Wang, X.; Zheng, J.; Sha, R.; Seeman, N. C. *Org. Biomol. Chem.* **2006**, *4*, 3414.
(20) Yan, H.; Park, S. H.; Finkelstein, G.; Reif, J. H.; LaBean, T. H. *Science* **2003**, *301*, 1882.
(21) Mathieu, F.; Liao, S.; Kopatsch, J.; Wang, T.; Mao, C.; Seeman, N. C. *Nano Lett.* **2005**, *5*, 661.
(22) He, Y.; Chen, Y.; Liu, H.; Ribbe, A. E.; Mao, C. *J. Am. Chem. Soc.* **2005**, *127*, 12202.
(23) He, Y.; Tian, Y.; Ribbe, A. E.; Mao, C. *J. Am. Chem. Soc.* **2006**, *128*, 15978.
(24) Malo, J.; Mitchell, J. C.; Turberfield, A. J. *J. Am. Chem. Soc.* **2009**, *131*, 13574.
(25) Liu, Y.; Ke, Y.; Yan, H. *J. Am. Chem. Soc.* **2005**, *127*, 17140.
(26) Mao, C.; Sun, W.; Seeman, N. C. *J. Am. Chem. Soc.* **1999**, *121*, 5437.
(27) Eichman, B. F.; Vargason, J. M.; Mooers, B. H. M.; Ho, P. S. *Proc. Natl. Acad. Sci. U. S. A.* **2000**, *97*, 3971.
(28) Timsit, Y.; Westhof, E.; Fuchs, R. P. P.; Moras, D. *Nature* **1989**, *341*, 459.
(29) Mao, C.; Sun, W.; Seeman, N. C. *J. Am. Chem. Soc.* **1999**, *121*, 5437.
(30) Otwinowski, Z.; Minor, W. *Methods Enzymol.* **1997**, *276*, 307.
(31) Pape, T.; Schneider, T. R. *J. Appl. Crystallogr.* **2004**, *37*, 843.
(32) Sheldrick, G. M. *Z. Kristallogr. - Cryst. Mater.* **2002**, *217*, 644.
(33) Uson, I.; Sheldrick, G. *Curr. Opin. Struct. Biol.* **1999**, *9*, 643.
(34) Adams, P. D.; Grosse-Kunstleve, R. W.; Hung, L. W.; Ioerger, T. R.; McCoy, A. J.; Moriarty, N. W.; Read, R. J.; Sacchettini, J. C.; Sauter, N. K.; Terwilliger, T. C. *Acta Crystallogr., Sect. D: Biol. Crystallogr.* **2002**, *58*, 1948.
(35) Terwilliger, T. C. *Methods Enzymol.* **2003**, *374*, 22.
(36) Emsley, P.; Cowtan, K. *Acta Crystallogr., Sect. D: Biol. Crystallogr.* **2004**, *60*, 2126.
(37) Murshudov, G. N.; Vagin, A. A.; Dodson, E. J. *Acta Crystallogr., Sect. D: Biol. Crystallogr.* **1997**, *53*, 240.
(38) Collaborative Computational Project, Number 4. *Acta Crystallogr., Sect. D: Biol. Crystallogr.* **1994**, *50*, 760−763.
(39) DeLano, W. L. *The PyMOL Molecular Graphics System*; DeLano Scientific: San Carlos, CA, 2002.

DOI: 10.1021/jacs.6b06508
J. Am. Chem. Soc. 2016, 138, 10047−10054